Glass transition of LiCl aqueous solutions confined in mesoporous silica

M. Paula Longinotti (iD), Violeta Fuentes-Landete, Thomas Loerting (iD), and Horacio R. Corti (iD)

View Online

Export Citation

CrossMark

ARTICLES YOU MAY BE INTERESTED IN

Submit Today

The Journal of Chemical Physics

The Emerging Investigators Special Collection and Awards
Recognizing the excellent work of early career researchers!

AIP Publishing

151, 064509

Glass transition of LiCl aqueous solutions confined in mesoporous silica

M. Paula Longinotti,[1] (iD) Violeta Fuentes-Landete,[2] Thomas Loerting,[2] (iD) and Horacio R. Corti[1,3,a] (iD)

AFFILIATIONS

[1] Instituto de Química Física de los Materiales, Medio Ambiente y Energía, Universidad de Buenos Aires, Ciudad Autónoma de Buenos Aires, Argentina
[2] Institute of Physical Chemistry, University of Innsbruck, Innrain 52c, 6020 Innsbruck, Austria
[3] Departamento de Física de la Materia Condensada, Comisión Nacional de Energía Atómica, San Martín, Buenos Aires, Argentina

Note: This paper is part of a JCP Special Topic on Chemical Physics of Supercooled Water.
[a] Author to whom correspondence should be addressed: hrcorti@cnea.gov.ar

ABSTRACT

The thermal transitions of confined LiCl aqueous solutions were studied by differential scanning calorimetry for solutions with salt concentrations with eutectic ($R = 7$) and subeutectic ($R > 7$) compositions (R = moles of water/moles of LiCl). The confinement media consist of mesoporous silica with pore diameters between 2 nm and 58 nm, with a small negative surface charge density. The vitrification of confined LiCl aqueous solutions was observed in all samples, expanding the vitrification region up to $R = 15$, and probably beyond for cooling rates of ≈1000 K/min. Ice crystallization was observed in some samples, except for those confined in the narrower pores. The onset and endpoint glass transition temperatures for the confined eutectic samples increase by 2 K and 5 K, respectively, for the smallest pore diameters (2 nm), which is equivalent to the effect of applying a pressure of up to 100 MPa to the bulk sample. This behavior is opposite of that reported for aqueous subeutectic NaCl solutions confined in silica glasses of similar sizes. We speculate that this is due to the fact that the mechanism of double confinement of the NaCl solution, between the pore wall and the precipitated ice, is not operative for LiCl solutions. Instead, the Li$^+$ ions might force the hydration water in to a high-density state.

Published under license by AIP Publishing. https://doi.org/10.1063/1.5102142

INTRODUCTION

The studies of phase transitions of aqueous solutions confined in nano- and mesopores are scarce. Findenegg and co-workers[1] studied the freezing and melting of aqueous solutions of potassium and sodium halides, and alkaline chlorides (except lithium) confined in cylindrical pores of MCM-41 (4.4 nm in diameter) and SBA-15 (7.1 nm and 8.5 nm in diameter) silica using differential scanning calorimetry (DSC). The results show a remarkable depression of the eutectic temperature of the confined solutions, particularly for salts that crystallize as oligohydrates at the eutectic point, since the precipitated salt results in an additional confinement for the solution inside the pores.

Wang and co-workers[2] found that subeutectic NaCl aqueous solutions, which are poor glass formers and only vitrify under pressure, can be vitrified all over the range of salt mole fractions ($0.0088 < x < 0.0826$) when confined in the narrower mesopores (2.6 nm and 5.7 nm) of silica-based porous glasses. However, in wider pores, only the more diluted solutions vitrify (for instance, $x < 0.023$ for pores 54 nm in diameter). Ice crystallizes at the center of the pore, enhancing the confinement of the residual eutectic phase located between the pore wall and the ice core, which only vitrifies when its thickness is below a critical value. No evidence of glass transition has been observed for KCl solutions confined in the same matrix.

The glass transition of glycerol aqueous solutions confined in MCM-41 silica with pores 2.1 nm in diameter was studied by Swenson and co-workers.[3,4] Contrary to that observed in confined ionic aqueous solutions, when mixed with glycerol, water molecules prefer to hydrate the silanol groups on the wall's pore

and a glycerol-rich solution is separated at the pore center, whose T_g is independent of the glycerol concentration up to a water concentration close to 85 wt. %.

In this work, we have undertaken a detailed DSC study of LiCl aqueous solutions confined in mesoporous silica over a wide range of pore sizes, ranging from 2 nm to 58 nm, in order to get a better understanding of the effect of confinement on the vitrification and crystallization of an ionic aqueous solution whose phase transition behavior in the bulk is well known.

The mesoporous silica is that employed in a previous study on the transport properties of confined electrolytes,[5] and its pore size range is quite similar to that of the silica matrices used by Wang and co-workers.[2] The microstructure of the silica used in this work resembles that of fumed silica, where confined water may show the least perturbation compared to bulk water.[6]

The range of salt concentration chosen for our study includes the bulk eutectic composition ($R = 7$, $x = 0.125$) and subeutectic solutions with R between 9 and 15 (see Table S1 in the supplementary material).

GLASS TRANSITION TEMPERATURE OF BULK LiCl/WATER SOLUTIONS

Before describing the calorimetric study of confined LiCl aqueous solutions, it is worth briefly summarizing the results reported in the literature for the thermal transitions of the LiCl/water bulk system.

The glass transition temperature of LiCl/water solutions was first reported by Angell and Sare,[7,8] by employing differential thermal analysis (DTA) in solutions with R in the range 1.7–11. By quenching in liquid nitrogen solutions with $9 < R < 11$, they observed a glass transition at 139 K, during the DTA warm-up, followed by a sudden crystallization at 152 K. When the sample was requenched in liquid nitrogen immediately after the crystallization peak, the glass transition is again observed at the same temperature. It was suggested that under cooling, the homogeneous solution splits into two phases, a water-rich and a salt-rich (salt hydrate) solution, near T_g. The unstable water-rich microdispersed glassy droplets cannot grow due to the low diffusivity and crystallize on warm-up.[7] T_g for LiCl aqueous solutions is almost identical to that of pure water (136 ± 2) K,[8,9] at salt concentrations lower than the eutectic composition ($R \approx 7$, $x \approx 0.125$), and increases monotonously from $R = 7$ up to 162 K for $R = 3$ ($x = 0.25$),[10] as it can be observed in the supplemented phase diagram shown in Fig. 1.[11]

Mayer and co-workers[12,13] determined the glass transition of dilute LiCl aqueous solutions ($x < 0.06$, $R > 15$) obtained by hyperquenching (cooling rate ≈ 10^6 K/s), followed by annealing at 123 K for 90 min. The scans display the endothermic glass to liquid transition and the beginning of an exothermic peak due to devitrification of cubic ice. The dependence of T_g on R (not shown in Fig. 1) is more complex than that observed at a higher salt concentration, including a minimum ($T_g \approx 129$ K) at $R \approx 42$, attributed to plasticization of the water's H-bonded network by the salt, and then T_g increases up to the values of concentrated aqueous solutions vitrified by slow cooling.

Kobayashi and Tanaka[14] performed a detailed study of the glass transition temperature of LiCl/water solutions over the concentration range $2.4 < R < 39$ ($0.025 < x < 0.294$) by resorting to
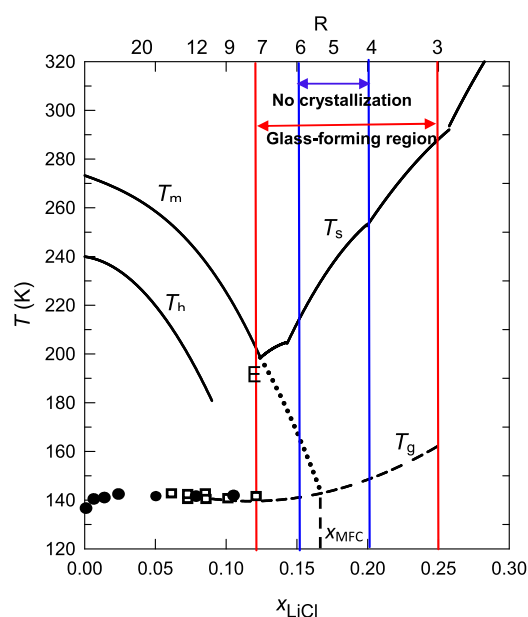

FIG. 1. Supplemented phase diagram of LiCl-water (adapted from Ref. 11), showing the ice melting curve (T_m), the LiCl solubility curve (T_s), the homogeneous nucleation curve (T_h), and the glass transition curve (T_g), including T_g determined in this work (□) and in a previous study (●).[18] The dotted line corresponds to the freezing evolution of a LiCl aqueous solution beyond the eutectic point (E), which finishes when the maximally freeze-concentrated solution (x_{MFC}) is reached.

temperature modulated DSC. The glass-forming ability is maximum in the region $4 < R < 6$ (blue lines in Fig. 1), where crystallization has never been observed even at cooling rates as low as 0.1 K/min. For $3 < R < 7$ (red lines in Fig. 1), a glass is also formed at cooling rates in the range 0.1–1 K/min, but crystallization sometimes takes place on heating above T_g, or even on cooling when the sample is cycled several times. The glass-forming region can extend up to $2.5 < R < 9$ if the cooling rate reaches values close to 20 K/min.

A link was proposed[15] between the V-shaped phase diagrams T vs x of the LiCl/water mixture and the T vs p diagram of pure water in such a way that the effect of adding salt to water is similar to applying pressure, that is, breaking the tetrahedral structure of water by formation of a hydration layer around the Li$^+$ ion.

The effect of pressure on T_g of LiCl aqueous solutions has also been studied up to 400 MPa for $R = 3$–10[16] and for $R = 8$–20,[17] and it was found that T_g increases between 3 and 5 K for each 100 MPa. Mishima obtained a similar pressure coefficient of T_g for emulsified LiCl aqueous solutions with $8 < R < 30$ at pressures up to 1 GPa.[18]

Further studies on the vitrification of LiCl aqueous solutions under pressure provide evidence of two different regimes. For LiCl aqueous solutions below $x = 0.10$ ($R \approx 9$), cooled down to 77 K at 0.3 GPa, there is a polyamorphic phase separation into low-density amorphous ice (LDA) and a glassy highly concentrated LiCl solution, whereas above $x = 0.10$, a glass-to-liquid transition is observed.[19] This behavior is the result of the formation of high-density amorphous water (HDA) near the Li$^+$ ion and supports the hypothesis by Mishima[18] that the effect of ion concentration is similar to the effect of pressure. In a previous study on pressure-induced

amorphization and polyamorphism in LiCl aqueous solutions,[9] we showed that unannealed HDA (uHDA) is formed by compression of LiCl solutions to 1.6 GPa at 77 K in the subeutectic concentration range ($x < 0.125$), as a result of the amorphization of segregated water.

A recent analysis of the water-dominated regime ($R > 7$) used a more complex sample preparation for HDA.[20] This route is necessary to remove seeds still present in uHDA that reduce the thermal stability.[21–23] Specifically, the preparation route involves high-pressure annealing (1.1 GPa) and high-temperature (140 K) decompression to relax the sample to form expanded HDA (eHDA). The higher thermal stability of eHDA allows us to reveal the existence of two glass transitions: first, the eHDA to HDL (high-density liquid) transition that takes place at around 116 K in pure water at a heating rate of 10 K/min.[24] The glass transition temperature shifts down to 110 K for heating rates of 0.01 K/min[24] and up to 125 K for heating rates of 50 K/min.[25] The presence of LiCl, however, does not shift water's second glass transition.[20] Second, the LDA to LDL (low-density liquid) glass transition occurs at 137 K for pure water, shifts to ≈140 K (prior to crystallization) for very dilute LiCl aqueous solutions ($x < 0.02$), and remains unaffected by a higher salt concentration (up to $x = 0.10$), as can be seen in Fig. 1.

The goal of the present study is to extend these studies and investigate under which conditions vitrification and/or crystallization takes place, where we work at higher cooling rates (of about 1000 K/min) and in different types of confinements down to 2 nm confinement. Also issues such as cold-crystallization upon heating and hence formation of crystallization seeds upon cooling are part of our study. To investigate the influence of the cooling rate alone, we also study samples by slowly cooling inside the DSC instrument at ≈3–4 K/min.

EXPERIMENTAL

Characterization of the mesoporous silica

Commercial mesoporous silica spheres CARIACT Q, 1–4 mm in diameter (provided by Fuji Silysia Chemical Ltd.), with nominal pore diameters between 3 and 30 nm were used in this study. A complete morphological and surface chemistry characterization of the materials has been reported recently in our previous study of the transport properties of alkaline chlorides under confinement.[5]

The specific surface area, the pore size distribution, and the average pore and neck diameters of the five mesoporous silica samples, determined from the nitrogen adsorption isotherm at 77 K (Micrometrics ASAP2020) using the Brunauer-Emmett-Teller

(BET) equation and density functional theory (DFT) from Micrometrics software, are summarized in Table I.

The pore wall of mesoporous silica is covered by silanol groups (–SiOH) that can dissociate or protonate depending on the pH of the media within the pore. The net surface charge density was determined by potentiometric titration, following the procedure reported in our previous work.[5]

Figure S2 in the supplementary material shows the results obtained for the Q30 sample as a function of pH, in the range between pH = 4 and pH = 7. The measured surface charge density is essentially zero (within an uncertainty of 0.005 C m^{-2}) in the range $4 < \text{pH} < 5.5$ and increases for pH > 5.5. A surface charge density of 0.005 C m^{-2}, which corresponds approximately to a pH close to that used in our measurements, between 5 and 6, implies the presence of an approximately elementary charge every 40 nm along the axial direction for the sample Q3, with a pore diameter of 2 nm.

Filling up the mesopores with LiCl aqueous solutions

In order to study the thermal transitions of LiCl aqueous solutions confined in the mesoporous matrices, the silica spheres were filled using the following procedure: (i) the mesoporous spheres were dried under vacuum at 120 °C overnight, to eliminate residual water, and weighed; (ii) the spheres were placed in a glass tube containing the corresponding LiCl aqueous solution, which was frozen by immersion in liquid nitrogen; (iii) the liquid nitrogen was then removed to allow the samples to slowly increase their temperature while being evacuated, for extracting the air in the silica pores; (iv) air at atmospheric pressure was finally allowed to enter into the system for forcing the LiCl solution to fill the silica pores; and (v) the sample was then superficially dried, using a tissue paper, and weighed. The mass difference of the sample after and before the filling process renders the mass of the solution inside the pores.

DSC measurements

The DSC thermal analysis was performed with a DSC PerkinElmer 4 (University of Innsbruck). Due to the size of the spheres, they were crushed into smaller pieces before placement in the DSC aluminum pans. The pans containing the confined samples were hermetically sealed and immersed in liquid nitrogen, before cold-loading them to the DSC kept at 93 K (protocol A). A sample cooling rate close to 1000 K/min was estimated upon immersing pans at room temperature in liquid nitrogen (77 K), considering that the nitrogen gas layer between the pan and the liquid (caused by the Leidenfrost effect) typically lasts between 10 and 13 s.

TABLE I. Pore diameter, d_{pore}, neck diameter, d_{neck}, pore volume, V_{pore}, specific area, SA, and porosity, ε, of the mesoporous silica samples.

Sample	d_{pore} (nm)	d_{neck} (nm)	V_{pore} (cm^{-3} g^{-1})	SA (m^2 g^{-1})	ε
Q3	2	2	0.29	540	0.38
Q6	8.0	5.5	0.62	391	0.57
Q10	20.4	10.6	1.00	297	0.68
Q15	38.3	18.8	0.98	188	0.67
Q30	57.7	31.3	0.91	95	0.66

The following protocol was employed for the DSC measurements: (i) first heating scan from 93 K to 213 K at 30 K/min; (ii) the sample was cooled from 213 K back to 93 K at 30 K/min; and (iii) a second heating scan was performed from 93 K to 303 K also at 30 K/min.

A second set of experiments were performed with a Mettler Toledo DSC (the University of Buenos Aires) by cooling the samples inside the equipment at a mean cooling rate of ≈3–4 K/min (the cooling rate was faster at the beginning and decreased as the sample approached the final temperature), followed by a heating scan from 133 K up to 303 K at 10 K/min (protocol B).

The high heating rate used in these protocols reduces the amount of ice formed due to cold-crystallization upon heating because the higher the heating rate, the lower the amount of ice formed in bulk samples,[26] criteria that could also be valid for confined samples.

RESULTS AND DISCUSSION

Figure 2 shows the DSC heating scans (after cooling the DSC crucibles in liquid nitrogen at about 1000 K/min) of aqueous solutions with $R = 7$, 9, 13, and 15, confined in silica mesoporous samples of different pore sizes. The base line, determined between 100 and 120 K, has been subtracted. The DSC scan of the bulk solution is included for comparison (red lines). A glass transition is clearly observed for all the samples, the onset of which occurs between 141.3 and 143.8 K for all compositions analyzed in this work. Only for the strongest confinement, in the Q3 silica samples, the onset shifts by around 2 K to higher temperatures.

For the samples with LiCl concentrations at the left of the eutectic point ($R > 7$), crystallization exothermic peaks are observed for some samples. For instance, for $R = 9$ [Fig. 2(b)], massive crystallization occurs in the bulk and the solutions confined in the mesoporous silica with larger pore sizes (Q15 and Q30), while it does not appear in the samples with smaller pores. These crystallization events represent cold-crystallization of the sample upon heating. Parts of the sample that vitrified upon cooling may exhibit such events. The nature of the cold-crystallization event is stochastic rather than determined by concentration or confinement. In Fig. 2, these events occur randomly at onset temperature between 160 and 175 K. The random nature can be seen best for $R = 9$ [Fig. 2(b)], in which Q30 confinement shows cold-crystallization at lower
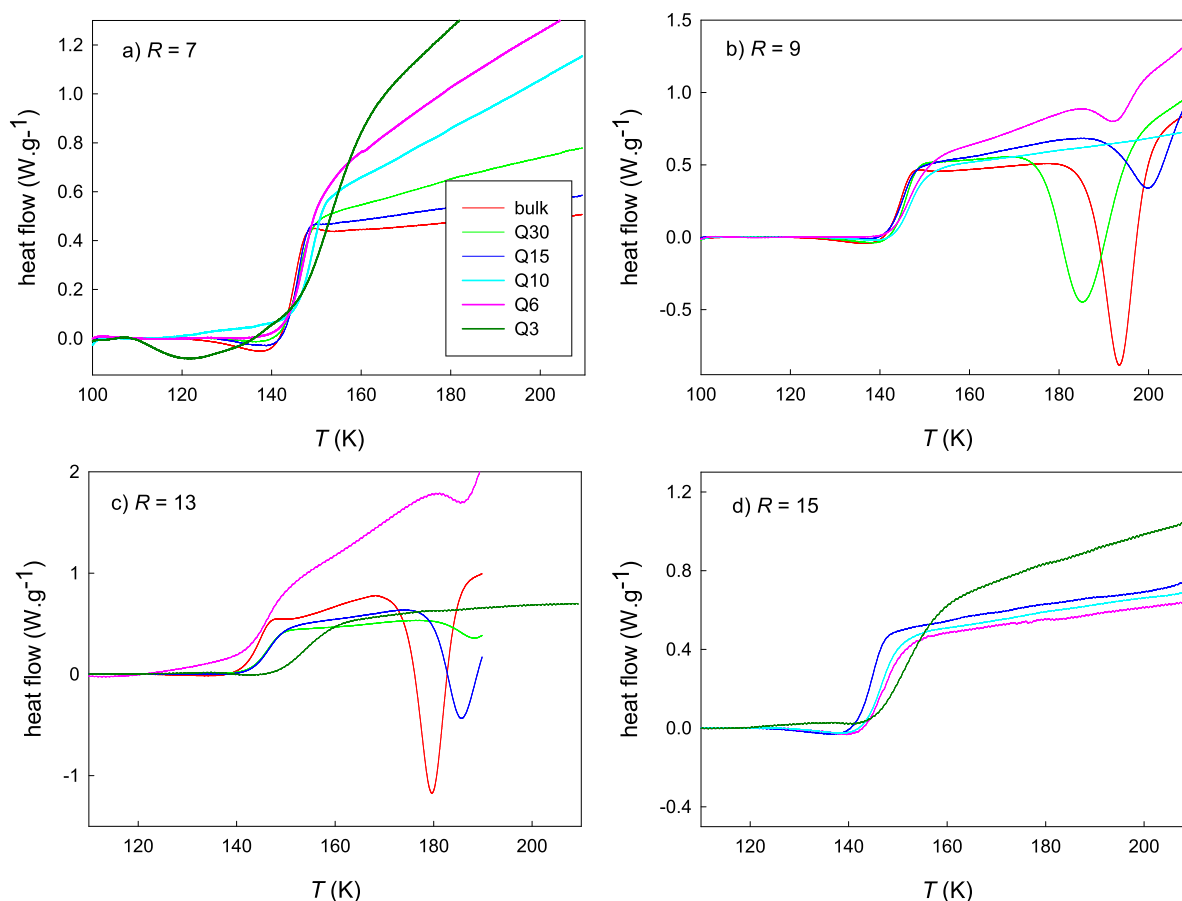

FIG. 2. First DSC heating scans of bulk and confined LiCl aqueous solutions with (a) $R = 7$, (b) $R = 9$, (c) $R = 13$, and (d) $R = 15$. Curves correspond to red (bulk), light green (Q30), blue (Q15), light blue (Q10), magenta (Q6), and green (Q3).

temperatures than in the bulk solution, whereas other confinements show cold-crystallization at higher temperatures. This stochastic nature of cold-crystallization reflects the well-known stochastic nature of nucleation upon cooling, which determines the nature of cold-crystallization in the subsequent heating scan.

For the samples with $R = 13$ [Fig. 2(c)], crystallization peaks are observed for the bulk and all the confined solutions, except for Q3. For the samples with $R = 15$ [Fig. 2(d)], crystallization peaks are not observed, just like for $R = 7$ [Fig. 2(a)]. That is, cold-crystallization is avoided for the severe confinement in Q3 in all cases. Also, for near-eutectic samples ($R = 7$), cold-crystallization is avoided, which reflects the known suppression of crystallization ability of eutectic mixtures. More surprisingly, cold-crystallization is avoided for water rich samples ($R = 15$), which might reflect the ability of the narrow pores (Q3–Q15) to suppress nucleation for dilute solutions. However, Q6 and Q15 pores do show cold-crystallization for $R = 9$ and $R = 13$ solutions.

The cooling scans from 213 K to 93 K, step (ii) of Protocol A, described previously are shown in Fig. 3, which details the cooling event after the heating scan shown in Fig. 2. The only thermal feature that is observed in Fig. 3 is the glass transition. The deeply supercooled liquid (at 200 K) never crystallizes upon cooling but rather vitrifies. The glass transition temperature is observed in the range 140–160 K for all samples. Change of concentration barely shifts the glass transition onset temperature T_g. Also, bulk samples and samples confined in Q30, Q15, and Q10 show very similar T_gs $\approx$ 145 K. For Q3 and Q6 confinements, however, T_g shifts to somewhat higher temperatures, $\approx$155 K. A similar shift of T_g to higher temperatures is also seen in Figs. 2(c) and 2(d) for Q3 confinement. In other words, the glass-to-liquid transition is reversible, where the parts cold-crystallized in the first heating scan do not show any thermal effects in the subsequent cooling run.

The second DSC heating scans shown in Fig. 4 again exhibit the glass transition, where its onset temperature increases with decreasing pore size, as reported in Table II and Table S2. The exothermic
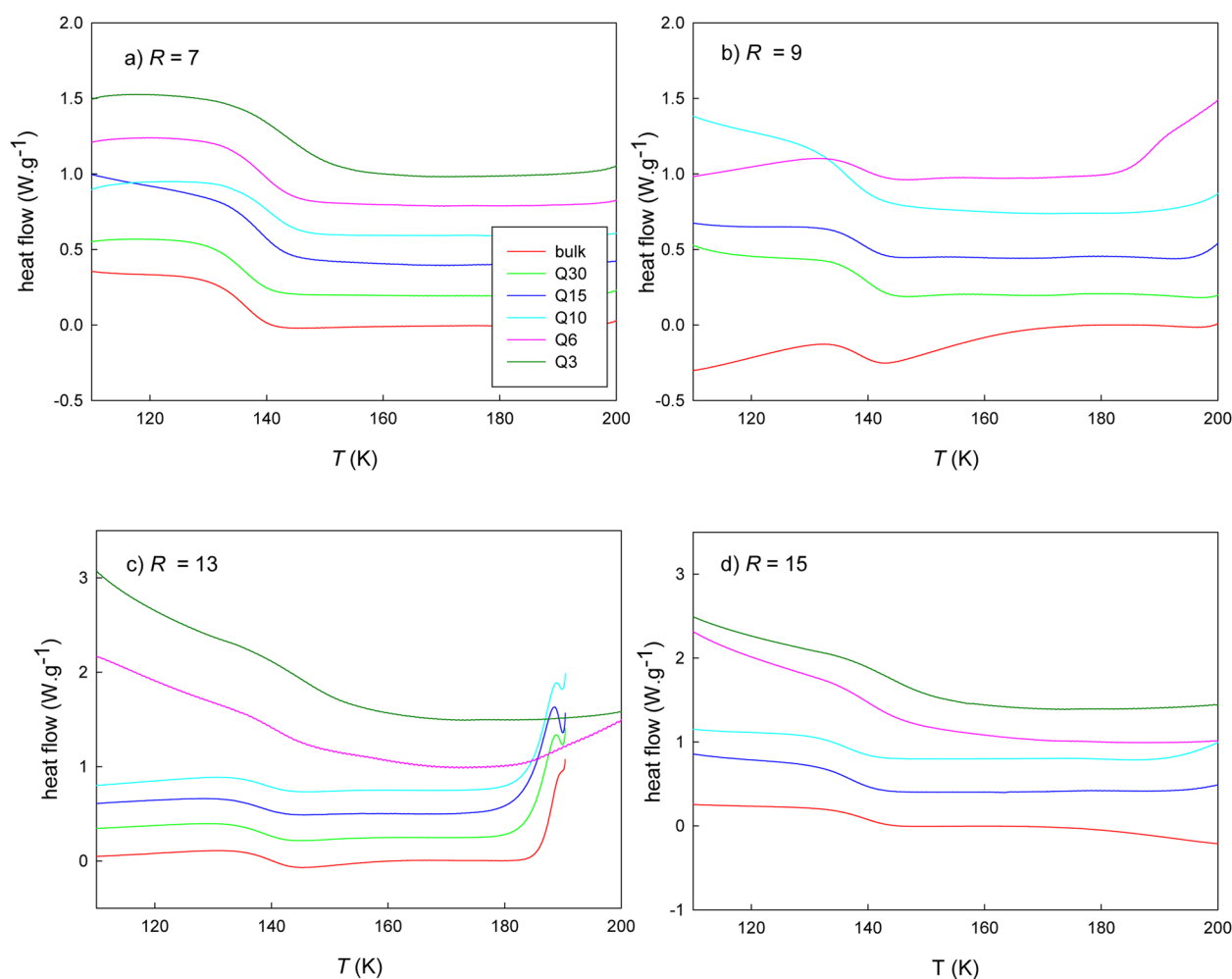

FIG. 3. Cooling DSC scans (at 30 K/min) of bulk and confined LiCl aqueous solutions with (a) $R = 7$, (b) $R = 9$, (c) $R = 13$, and (d) $R = 15$. Curves' color as in Fig. 2. The cooling scans were conducted immediately after the heating scans shown in Fig. 2 (starting from 213 K).
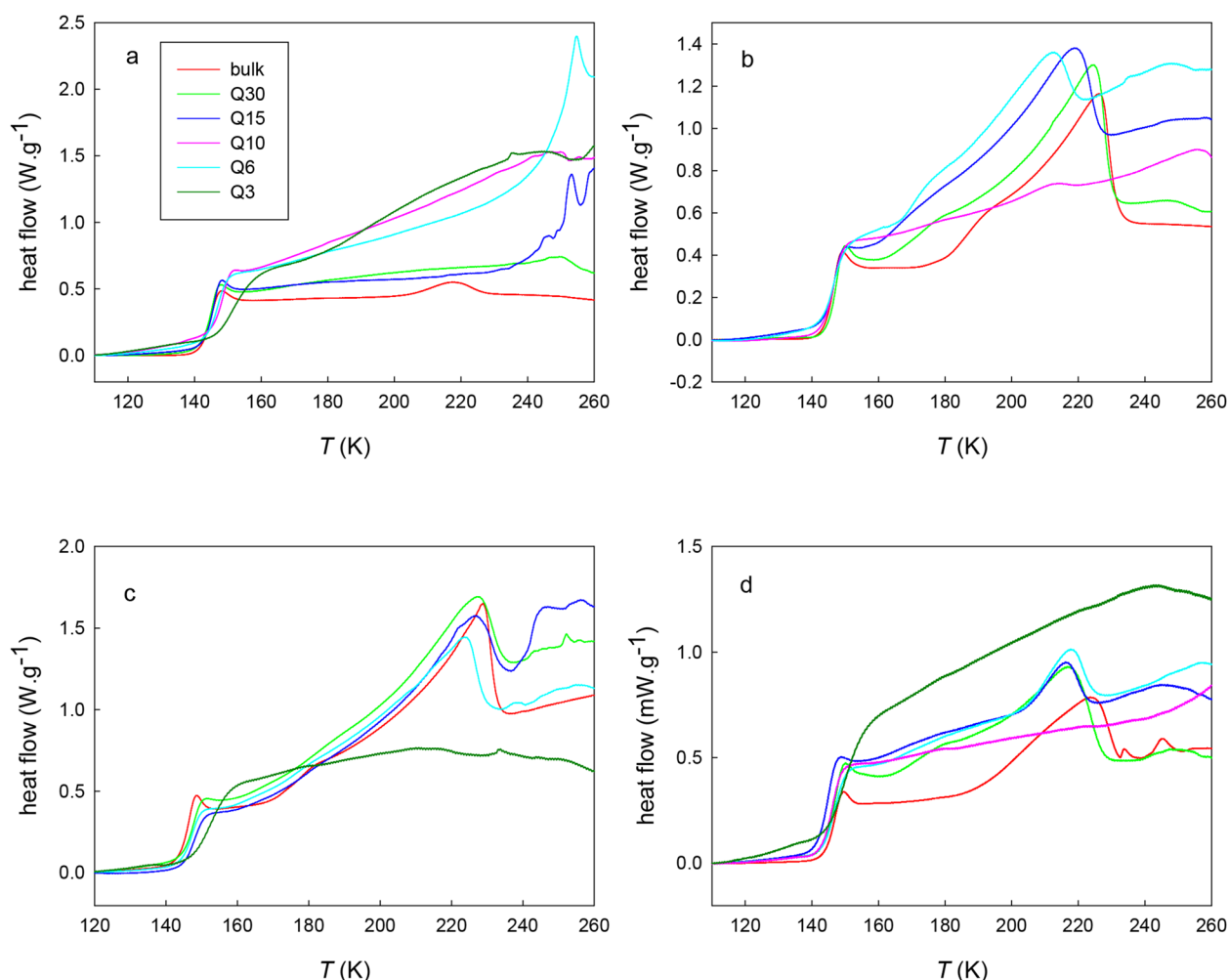
FIG. 4. Second DSC heating scans (at 30 K/min) of bulk and confined LiCl aqueous solutions with (a) $R = 7$, (b) $R = 9$, (c) $R = 13$, and (d) $R = 15$. Curves' color as in Fig. 2.

cold-crystallization events are absent in these thermograms. This is expected since cold-crystallization has already taken place in the first heating scan. Since the second heating scan brings the sample beyond 213 K (by contrast to the first heating scan in Fig. 2), additional thermal events are recorded. The crystalline fraction of these samples is evidenced above 213 K by a number of endothermic peaks in Fig. 4 pertaining to the melting events of the crystalline parts.

For the bulk sample at the eutectic composition [$R = 7$, Fig. 4(a)], a small endotherm is observed at ∼210 K, close to the eutectic temperature, probably due to the melting of a small fraction of the solution that crystallized, instead of vitrifying. For samples confined in the large pore silica (Q30, Q15, Q10, and Q6), the endothermic peaks are multiple and shift to higher temperatures (>240 K), while for the smallest pore sample (Q3), there are no endothermic peaks. This behavior can be explained considering that confinement in silica induces concentration heterogeneities in the region close to the wall and the center of the pore, which

split the eutectic composition into solutions having concentrations above and below the eutectic one, leading to the crystallization of ice and maximally freeze-concentrated solution upon cooling, that melt during the second heating scan. This type of heterogeneity could not be developed in the solution confined in the Q3 mesopores having the smallest pore size, where ice crystallization is inhibited for solutions with R between 7 and 13.

For solutions with lower LiCl content than the eutectic composition [Figs. 4(b)–4(d), $R > 7$], the second scan curves exhibit endothermic peaks at temperatures between 210 K and 250 K that can be attributed to the melting of the eutectic or the maximally freeze-concentrated solutions formed during the quenching down to 93 K. These melting peaks are all asymmetric, with a long tail on the low-temperature side. This tail indicates that the melting of ice changes the composition of the solution, thereby shifting the melting temperature. This is typical of binary solutions with water, where first and last melting temperatures are observed. The exception is again the Q3 sample, for which just vitrification and devitrification

TABLE II. Onset and endpoint glass transition temperatures, width of the transition, and change of heat capacity (per gram of water) at T_g for aqueous LiCl solutions with $R = 7$. The results for the second scan are shown within parenthesis.

Sample	$T_{g,onset}$ (K)	$T_{g,end}$ (K)	$100\, \Delta T_g/T_{g,onset}$	ΔC_p (J/g K)
Bulk	142.3 (141.5)	147.4 (146.5)	3.6 (3.6)	1.14 (1.07)
Q30	142.6 (141.6)	149.4 (146.4)	4.8 (3.4)	1.34 (1.15)
Q15	143.3 (142.3)	147.9 (147.1)	3.2 (3.4)	1.20 (1.15)
Q10	145.5 (145.2)	152.0 (150.0)	4.5 (3.3)	1.34 (1.12)
Q6	143.4 (143.4)	151.0 (149.5)	5.3 (4.3)	1.70 (1.31)
Q3	144.4 (146.5)	163.0 (157.7)	12.9 (7.6)	2.40 (1.24)

are observed. That is, extreme confinement prohibits crystallization, while crystallization can take place for samples in bulk or confined in large pores.

Figure 5 shows the onset glass transition temperatures, the width of the glass transition expressed as $100\, \Delta T_g/T_{g,onset}$, where $\Delta T_g = T_{g,end} - T_{g,onset}$, and the change of heat capacity, ΔC_p, for the glass transition for all LiCl aqueous solutions studied in this work.

In Fig. 5, it can be observed that $T_{g,onset}$ slightly increases with decreasing pore size, since for the larger pores $T_{g,onset} = (143 \pm 2)$ K increasing this value to (146 ± 2) K for the solutions confined in smaller pores. It can be clearly observed that the width of the glass transition increases with decreasing pore size from about 4% to about 8%, independent of the LiCl concentration. The variation of the glass transition width with a concentration at a given pore size
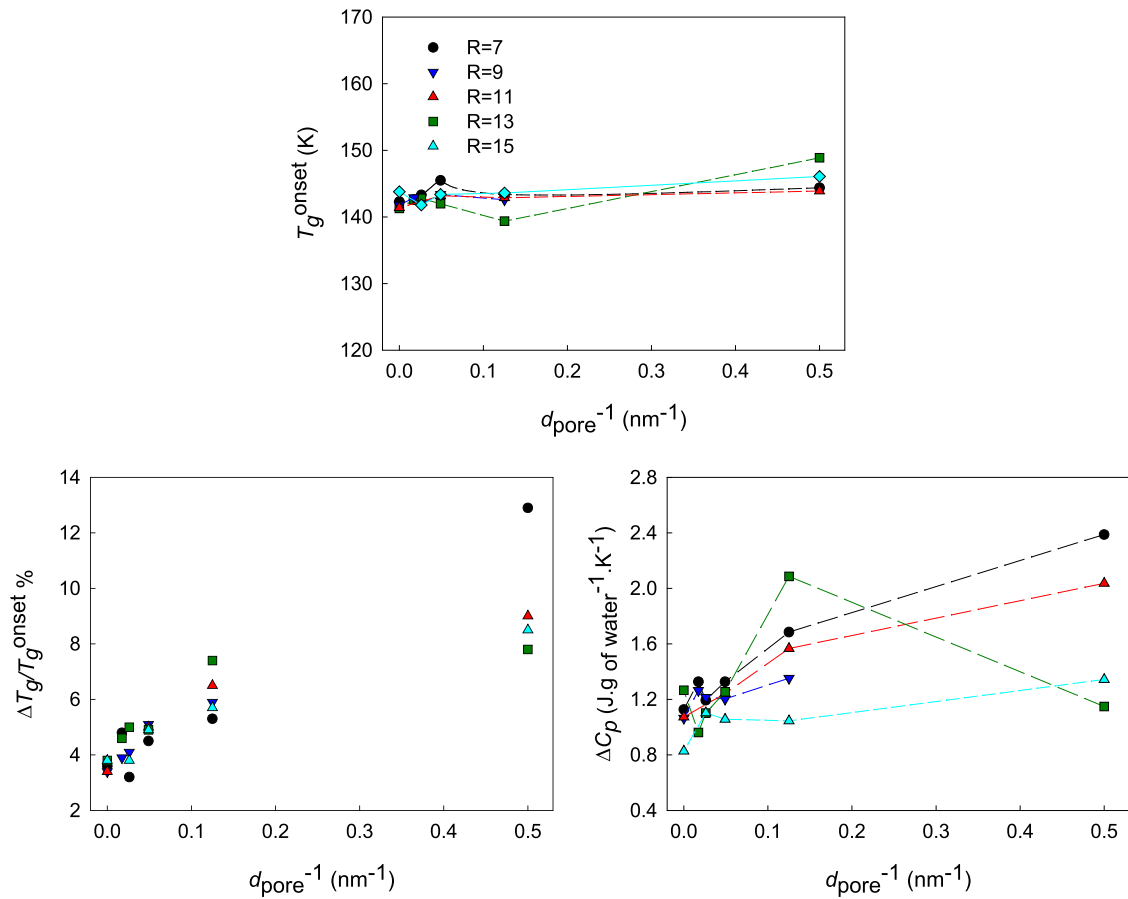

FIG. 5. Onset glass transition temperatures $T_{g,onset}$, width of the glass transition $100\, \Delta T_g/T_{g,onset}$, and change of heat capacity ΔC_p for the glass transition for all LiCl aqueous solutions studied in this work plotted against inverse pore diameter.

is small (±1%), in contrast. The sample Q3 with $R = 7$ is an exception because the width of the glass transition increases from 8% up to 13%. Moreover, ΔC_p (given per gram of water) is around 1.1 J g^{-1} K^{-1} for bulk and large pores. For small pores, this value is slightly higher, but never above 2.4 J g^{-1} K^{-1}.

Turning back to the glass transitions observed during the first and second heating scans, Table II summarizes the results obtained for the onset and endpoint glass transition temperatures, the width of the glass transition, expressed as $100 \, \Delta T_g / T_{g,onset}$, where $\Delta T_g = T_{g,end} - T_{g,onset}$, and the calculated change of heat capacity for the glass transition for the samples with $R = 7$ (eutectic composition).

There is a good agreement between the onset glass transition temperatures for both scans, while for the endpoint temperature, the second scan shows temperatures lower by between 1 K and 5 K than the first scan. This is because the fictive temperature is higher for the samples before the first scan (previously cooled at 1000 K/min) in Fig. 2 than that for the samples before the second scan (previously cooled at 30 K/min) in Fig. 4. The excess entropy in these glasses is also higher, making the glass transition broader. ΔC_p seems to increase for the solutions confined in the smaller pores (Q6 and Q3), but this behavior is not so evident for the second scan and decreases for all the samples in the second scan. This again reflects that a small fraction of the sample vitrifies before the second scan, reducing the magnitude of the heat capacity change. One additional difference between the fast and slow cooled samples is the overshoot effect. The overshoot effect is more pronounced in Fig. 4 than in Fig. 2. This is in full accordance with the expectations. As outlined by Moynihan and co-workers[27–29] for a fast cooling rate and a comparably small heating rate, one expects undershoots, as seen in Fig. 2. However, if the heating rate is faster or similar to the cooling rate, one expects overshoots as seen in Fig. 4. The change of heat capacity during the glass transition is of the order of 20 J mol$_{water}$$^{-1}$ K^{-1} or higher, which are values similar to those observed for the first glass transition (LDA to LDL) in the LiCl solutions vitrified by high pressure compression.[24]

Generally speaking, the differences between the onset and the end point and ΔC_p of the transition also increase with decreasing pore size and can be related to a decrement in the fragility of the LiCl solutions with decreasing pore size. These changes can be noticed especially for the narrower pores, Q3 and Q6.

An alternative way of analyzing the results is presented below, where the thermograms obtained for samples with different R values confined in mesoporous silica, for both cooling and heating protocols (A and B), are compared.

Figure 6 shows the scans performed with protocols A (second heating scan) and B for LiCl solutions confined in Q3 silica. $T_{g,onset}$ are in good agreement in both cases within the experimental error (±1 K). A melting peak (not shown in the figure) is observed using protocol B, with an onset at 207 K and a peak at 221 K, for the sample with $R = 13$. The onset melting temperature is lower than the corresponding equilibrium melting temperature of ice for that composition, but close to the melting temperature of the eutectic composition. Thus, it can be hypothesized that in this case during cooling the sample, the eutectic composition or that of the maximally freezing concentration solution is attained. In protocol B, the cooling rate before the scan is even slower than the one before for the second scan in protocol A. Although the observed glass transition would correspond to that solution, its value is similar to the values measured for the eutectic composition, as can be seen in Fig. 1. However, as shown in Fig. 1, for $R > 7$, T_g of bulk samples does not vary much with the concentration for $R > 7$. Thus, it seems reasonable that this also occurs for confined samples.

Figures 7(a) and 7(b) show the scans using protocol A (second heating scan) and protocol B, respectively, for solutions confined in the Q10 silica. For the first scan with protocol A (heating rate 30 K/min), the solutions with $R = 7$ and $R = 9$ do not exhibit crystallization peaks. With a lower heating rate (protocol B), crystallization can be inferred for $R = 13$ because a melting peak with an onset around 200K is observed upon heating [Fig. 7(b)], just like for protocol A [Fig. 7(a)].
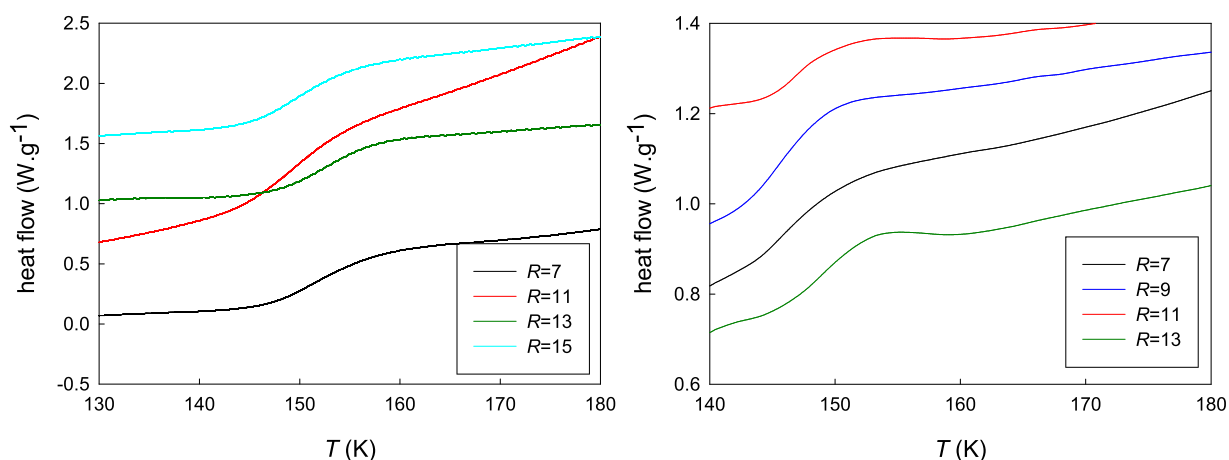

FIG. 6. DSC heating scan of LiCl confined in Q3 silica using protocol A at 30 K/min (left) and protocol B at 10 K/min (right). The previous cooling rates are 30 K/min (left) and 3–4 K/min (right). Curves: $R = 7$, black; $R = 9$, blue; $R = 11$, red; $R = 13$, green; and $R = 15$, light blue.
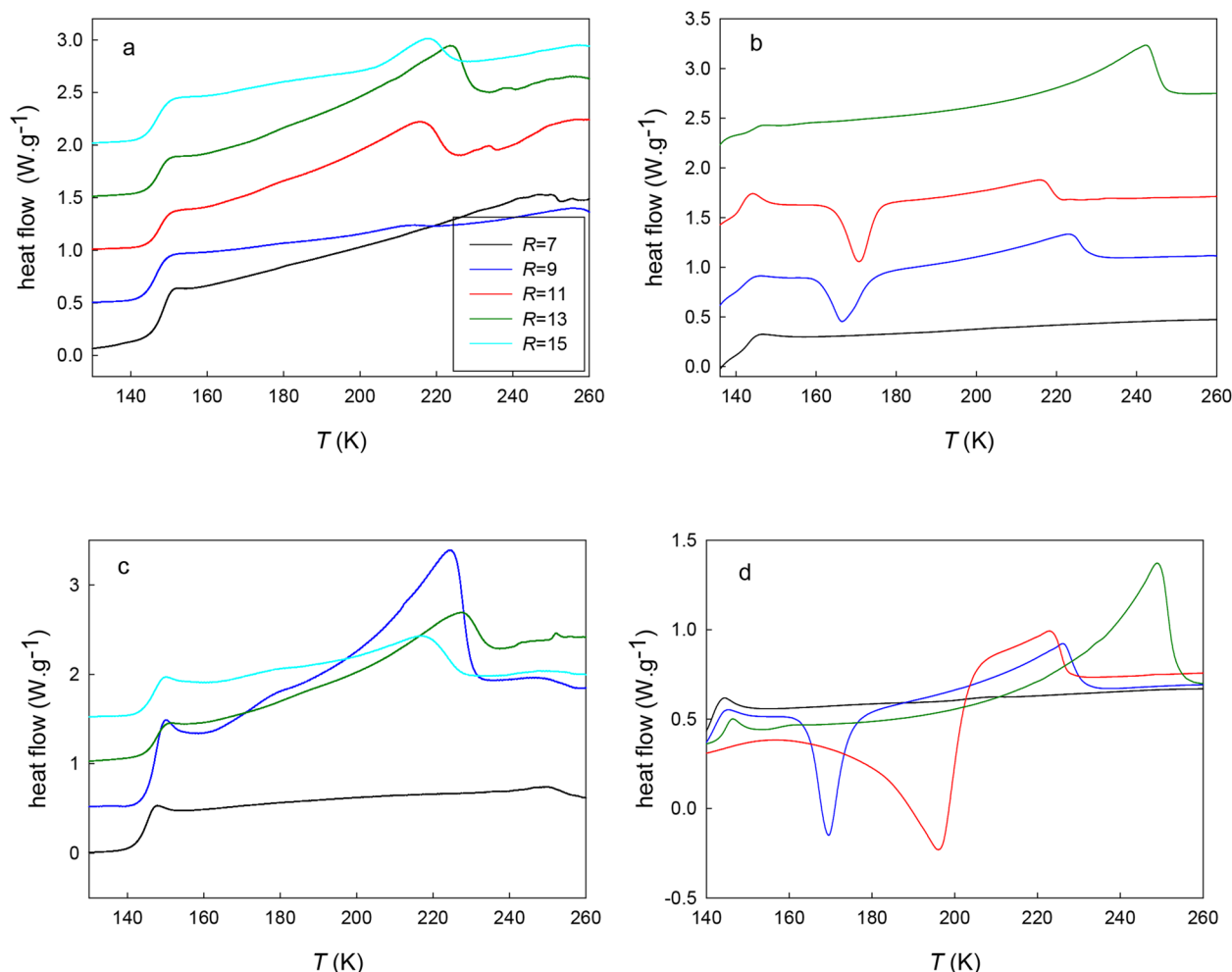
FIG. 7. DSC heating scans for LiCl confined in Q10 [(a) and (b)] and Q30 [(c) and (d)] silica using protocol A [(a) and (c)] and protocol B [(b) and (d)]. Curves: $R = 7$, black; $R = 9$, blue; $R = 11$, red; $R = 13$, green; and $R = 15$, light blue.

This behavior is confirmed for solutions confined in Q30 silica [Figs. 7(c) and 7(d)], where crystallization takes place for solutions with $R = 9$ and $R = 11$, while for $R = 13$, crystallization occurs during the initial cooling of the sample. Consequently, a slow cooling rate of 3–4 K/min (protocol B) results in crystallization already upon cooling ($R = 13$) or in cold-crystallization upon reheating ($R = 9$ and $R = 11$). Only for the eutectic composition of $R = 7$, full vitrification is possible at slow rates. This reflects the well-known tendency of glass-forming ability being highest for the eutectic composition and lowest in dilute solutions and pure water. A cooling rate of 1000 K/min (protocol A), by contrast, however, is high enough to prevent crystallization or nucleation upon cooling in most cases. Only in some selected cases (see Fig. 2), cold-crystallization takes place for solutions cooled at 1000 K/min, mainly for larger pores, $R = 9$, and $R = 13$.

The melting observed for the LiCl solution with $R = 9$ confined in silica Q10 and Q30 occurs at 166 K and 170 K, respectively, that

is, at 32 K and 28 K below the melting of the bulk. For the solution with $R = 11$, the depression of the eutectic melting point reaches 28 K in silica Q10 but is small in silica Q30. The shift of the melting temperature is of the same magnitude as that found by Findenegg and co-workers[1] for other alkaline chlorides (excluding LiCl), even when the pore size of the Q10 and Q30 silica is much larger. For LiCl confined in silica Q3 and Q6, with a similar pore size to that of MCM-41 and SBA-15, no crystallization is observed for samples with $R = 9$ and $R = 11$, but the sample with $R = 13$ seems to crystallize during the cooling scan and it melts close to the temperature of the eutectic point on heating. Thus, the freezing/melting pattern for LiCl aqueous solutions is much more complex than that of NaCl because of its tendency to vitrify that is enhanced in mesoporous silica.

In summary, for LiCl aqueous solutions confined in mesoporous silica, vitrification is observed in all cases. Ice crystallizes in some samples during cooling (by quenching in liquid nitrogen or at

a lower cooling rate), where lower salt concentrations (higher R) are needed for this to occur in narrower pores.

It is worth noting that for aqueous NaCl solutions confined in silica glasses, T_g decreases with decreasing pore size.[2] The differences in T_g between solutions confined in 54.0 nm pores (which are supposed to behave almost as in the bulk) and in the smallest pores (2.6 nm in diameter) are close to 20 K for the dilute solutions ($0.0088 < x < 0.0265$).[2] The decrease in T_g for the concentrated solutions ($x > 0.0265$) is not clear because the glass transitions of these solutions for the wider mesoporous glasses were not reported. The opposite behavior of T_g with the size of the pores for NaCl and LiCl could be due to the tendency of NaCl to segregate water upon cooling, leading to a eutectic solution that forms a layer on the pore wall, whose thickness is determined by the amount of ice in the pore core. Zhao et al.[2] proposed that the NaCl eutectic solution is doubly confined, by the wall pore and the ice core, and the decrease of T_g with decreasing pore size is related to the fact that for wider pores, more ice is formed and the eutectic layer becomes thinner than the eutectic confined in narrower pores. Moreover, differences in the ion-wall interactions for both aqueous mixtures can play a role in the confinement effect on T_g.

Finally, it is interesting to compare the glass-forming concentration range for bulk LiCl aqueous solutions with that observed for other confined samples. Figure 1 shows that, in previous studies, bulk LiCl solutions can be vitrified within the interval $R = 3$–7 at moderated cooling rates and that the interval expands up to $R = 2.5$–9 by cooling at 20 K/min. Here, by cooling at 30 K/min, we could vitrify solutions up to $R = 15$ even in the bulk, although in this case, and for the solutions confined in the wider pores, the separation of ice is observed and the measured T_g corresponds to the eutectic or the maximally freeze-concentrated solutions. For the smallest pore silica (Q3), there is no doubt that vitrification of the LiCl solution with $R > 7$ occurs without ice separation.

Thus, confinement in pores of sizes in the order of a few nanometers allowed us to study dilute LiCl solutions (subeutectic or water-dominated region) that, so far, were only accessible by amorphization at very high pressures.[18]

CONCLUSIONS

The glass transition temperature of LiCl aqueous solutions with composition in the range $7 < R < 15$ has been measured in mesoporous silica with pore sizes in the range between 2 nm and 58 nm. The vitrification of LiCl aqueous solutions confined in mesoporous silica is observed in all cases. For the very fast cooling rate (protocol A), there is no crystallization (other than nanocrystal formation beyond the detection limit of the instrument) upon cooling before the first scan because no melting endotherms are seen in heating scans. The problems about ice crystallization only appear when the liquid solution is cooled inside the DSC (protocol B) instead of plunging a DSC capsule into liquid nitrogen. Thus, the first scan for protocol A renders the "real" T_g of the solution and is not affected by freeze-crystallization. Interestingly, the glass transition temperature barely changes with the type of confinement and is found in the range of 140–145 K for all concentrations and types of confinements studied (see Fig. 5). For the confined samples with the eutectic composition ($R = 7$), the onset and endpoint glass transition temperatures increase with decreasing pore size. For the smallest pore

diameter (2 nm), the onset and endpoint temperatures increase by 2 K and 5 K, respectively, which is equivalent to the effect of applying a pressure around 100 MPa to the bulk sample.

This is in stark contrast with the situation in confined NaCl solutions, for which a T_g decrease of 20 K was reported for similar types of confinements ranging between 2.6 nm and 54 nm.[2] One may speculate that this is the case because the mechanism envisioned by Wang and co-workers[2] of double confinement of the solution between pore wall and precipitated ice is not operative for LiCl solutions. Indeed, our results show that ice crystallization is suppressed at a cooling rate of 1000 K/min. No ice separation is observed for the LiCl solutions confined in the narrower pores, expanding the vitrification region up to $R = 15$, and probably beyond, a composition that can only be achieved by amorphization of the solutions at very high pressures. However, the glass transition temperature also remains near 140 K for solutions cooled at 3–4 K/min, for which ice formation is observed [see Figs. 7(b) and 7(d)]. In other words, the formation of ice and freeze-concentrated LiCl solutions does not result in a shift of T_g either. The remarkable stability of the T_g might instead point toward phase segregation in the liquid solution into a LiCl-rich and LiCl-poor solution, as also envisioned by Suzuki and Mishima in their work on bulk samples.[19] The hydration water might be HDA-like for the LiCl-rich part, and this might explain why T_g does not shift. Only for the most diluted solutions ($R > 7$), the confinement effect on the glass transition temperature seems to be present, but only in the sample with the narrowest pores. This might imply that phase segregation in the liquid state is harder to achieve or even to suppress for 2 nm confinement, in contrast to the larger confinement.

SUPPLEMENTARY MATERIAL

See supplementary material for details of the morphological and surface chemistry characterization of the mesoporous silica, glass transition temperatures, and changes of heat capacity of confined LiCl aqueous solutions with $R > 7$.

REFERENCES

[1] J. Meissner, A. Prause, and G. H. Findenegg, "Secondary confinement of water observed in eutectic melting of aqueous salt systems in nanopores," J. Phys. Chem. Lett. **7**, 1816–1820 (2016).

[2] L. Zhao, L. Pan, Z. Cao, and Q. Wang, "Confinement-induced vitrification of aqueous sodium chloride solutions," Chem. Phys. Lett. **647**, 170–174 (2016).

[3] J. Swenson, K. Elamin, H. Jansson, and S. Kittaka, "Why is there no clear glass transition of confined water?," Chem. Phys. **424**, 20–25 (2013).

[4] K. Elamin, H. Jansson, S. Kittaka, and J. Swenson, "Different behavior of water in confined solutions of high and low solute concentrations," Phys. Chem. Chem. Phys. **15**, 18437–18444 (2013).

[5] D. C. Martínez Casillas, M. P. Longinotti, M. M. Bruno, F. Vaca Chávez, R. H. Acosta, and H. R. Corti, "Diffusion of water and electrolytes in mesoporous silica with a wide range of pore sizes," J. Phys. Chem. C **122**, 3638–3647 (2018).

[6] A. Bogdan and T. Loerting, "Phase separation during freezing upon warming of aqueous solutions," J. Chem. Phys. **141**, 18C533 (2014).

[7] C. A. Angell and E. J. Sare, "Liquid-liquid inmiscibility in common aqueous salt solutions at low temperatures," J. Chem. Phys. **49**, 4713–4714 (1968).

[8] I. Kohl, L. Bachmann, E. Mayer, A. Hallbrucker, and T. Loerting, "Liquid-like relaxation in hyperquenched water at T < 140 K," Phys. Chem. Chem. Phys. **7**, 3210–3220 (2005).

[9] K. Amann-Winkel, R. Böhmer, F. Fujara, C. Gainaru, B. Geil, and T. Loerting, "Colloquium: Water's controversial glass transitions," Rev. Mod. Phys. **88**, 011002 (2016).

[10] C. A. Angell and E. J. Sare, "Glass forming composition regions and glass transition temperatures of aqueous electrolyte solutions," J. Chem. Phys. **52**, 1058–1068 (1970).

[11] G. N. Ruiz, L. E. Bove, H. R. Corti, and T. Loerting, "Pressure-induced transformations in aqueous LiCl solutions at 77 K," Phys. Chem. Chem. Phys. **16**, 18553–18562 (2014).

[12] K. Hofer, A. Hallbrucker, E. Mayer, and G. P. Johari, "Vitrified dilute aqueous solutions. 3. Plasticization of water's H-bonded network and the glass transition temperature's minimum," J. Phys. Chem. **93**, 4674–4677 (1989).

[13] K. Hofer, G. Astl, E. Mayer, and G. P. Johari, "Vitrified dilute aqueous solutions. 4. Effects of electrolytes and polyhydric alcohols on the glass transition features of hyperquenched aqueous solutions," J. Phys. Chem. **95**, 10777–10781 (1991).

[14] M. Kobayashi and H. Tanaka, "Relationship between the phase diagram, the glass-forming ability, and the fragility of a water/salt mixture," J. Phys. Chem. B **115**, 14077–14090 (2011).

[15] M. Kobayashi and H. Tanaka, "Possible link of the V-shaped phase diagram of the glass-forming ability and fragility in a water/salt mixture," Phys. Rev. Lett. **106**, 125703 (2011).

[16] D. R. MacFarlane, J. Scheirer, and S. I. Smedley, "Pressure coefficients of conductance and of glass transition temperature in concentrated LiCl, LiI and AlCl$_3$ solutions," J. Phys. Chem. **90**, 2168–2173 (1986).

[17] H. Kanno, "Double glass transition in aqueous lithium chloride solutions vitrified at high pressures: Evidence for a liquid-liquid-immiscibility," J. Phys. Chem. **91**, 1967–1971 (1987).

[18] O. Mishima, "The glass-to-liquid transition of the emulsified high-density amorphous ice made by pressure-induced amorphization," J. Chem. Phys. **121**, 3161–3164 (2004).

[19] Y. Suzuki and O. Mishima, "Sudden switchover between the polyamorphic phase separation and the glass transition in glassy LiCl aqueous solutions," J. Chem. Phys. **138**, 084507 (2013).

[20] G. N. Ruiz, K. Amann-Winkel, L. E. Bove, H. R. Corti, and T. Loerting, "Calorimetric study of water's two glass transitions in the presence of LiCl," Phys. Chem. Chem. Phys. **20**, 6401–6408 (2018).

[21] J. Stern, M. Seidl-Nigsch, and T. Loerting, "Evidence for high-density liquid water between 0.1 and 0.3 GPa near 150 K," Proc. Natl. Acad. Sci. U. S. A. **116**, 9191–9196 (2019).

[22] C. M. Tonauer, M. Seidl-Nigsch, and T. Loerting, "High-density amorphous ice: Nucleation of nanosized low-density amorphous ice," J. Phys.: Condens. Matter **30**, 034002 (2018).

[23] M. Seidl, A. Fayter, J. N. Stern, G. Zifferer, and T. Loerting, "Shrinking water's no man's land by lifting its low-temperature boundary," Phys. Rev. B **91**, 144201 (2015).

[24] K. Amann-Winkel, C. Gainaru, P. H. Handle, M. Seidl, H. Nelson, R. Böhmer, and T. Loerting, "Water's second glass transition," Proc. Natl. Acad. Sci. U. S. A. **110**, 17720–17725 (2013).

[25] V. Fuentes-Landete, L. J. Plaga, M. Keppler, R. Böhmer, and T. Loerting, "Nature of water's second glass transition elucidated by doping and isotope substitution experiments," Phys. Rev. X **9**, 011015 (2019).

[26] D. R. MacFarlane and M. Fragoulis, "Theory of devitrification in multicomponent glass forming systems under diffusion control," Phys. Chem. Glasses **27**, 228–234 (1986).

[27] C. T. Moynihan, A. J. Easteal, M. A. De Bolt, and J. Tucker, "Dependence of the fictive temperature of glass on cooling rate," J. Am. Ceram. Soc. **59**, 12–16 (1976).

[28] M. A. DeBolt, A. J. Easteal, P. B. Macedo, and C. T. Moynihan, "Analysis of structural relaxation in glass using rate heating data," J. Am. Ceram. Soc. **59**, 16–21 (1976).

[29] A. J. Easteal, J. A. Wilder, R. K. Mohr, and C. T. Moynihan, "Heat capacity and structural relaxation of enthalpy in As$_2$Se$_3$ glass," J. Am. Ceram. Soc. **60**, 134–138 (1977).